Pure Water Splitting Driven by Overlapping Electric Double Layers

Haosen Xu,[1,2] Jianbo Zhang, [1,*] Michael Eikerling,[2,3] Jun Huang,[2,4,*]

1 School of Vehicle and Mobility, State Key Laboratory of Automotive Safety and Energy, Tsinghua University, 100084, Beijing, China

2 IEK-13, Institute of Energy and Climate Research, Forschungszentrum Jülich GmbH, 52425, Jülich, Germany

3 Chair of Theory and Computation of Energy Materials, Faculty of Georesources and Materials Engineering, RWTH Aachen University, 52062, Aachen, Germany

4 Theory of Electrocatalytic Interfaces, Faculty of Georesources and Materials Engineering, RWTH Aachen University, 52062, Aachen, Germany

** Corresponding author, e-mail: ju.huang@fz-juelich.de, jbzhang@tsinghua.edu.cn*

Abstract

In pursuit of a sustainable future powered by renewable energy, hydrogen production through water splitting should achieve high energy efficiency with economical materials. Here, we present a nanofluidic electrolyzer that leverages overlapping cathode and anode electric double layers (EDLs) to drive the splitting of pure water. The strong electric field within the overlapping EDLs enhances ion migration and facilitates the dissociation of water molecules. Acidic and basic environments, that are created *in situ* at cathode and anode, respectively, enable the use of non-precious metal catalysts. All these merits allow the reactor to exhibit a current density of 2.8 $A \cdot cm^{-2}$ at 1.7 V with a nickel anode. This paves the way towards a new type of water electrolyzers without membranes, supporting electrolytes, or precious metal catalysts.

Introduction

A defossilized global energy ecosystem hinges on deploying renewable energy sources like solar and wind power (*1*). Hydrogen (H_2) emerges as a leading energy storage medium to mitigate the fluctuations and temporal-spatial distributions inherent in renewable energy harvesting (*2*). Powered by cheap electricity from renewable sources, electrochemical water splitting is considered to be a clean, affordable, and scalable way of green H_2 production. However, insufficient energy efficiency and high material costs remain major obstacles to the large-scale deployment of water electrolysis. The challenge is further exacerbated by the fluctuating nature of renewable energy, which limits the operation time of water electrolyzers at full capacity (*3*).

Despite significant progress in water electrolysis technologies, existing variants still fall short in meeting target metrics, either in terms of energy efficiency or cost-effectiveness. Alkaline water electrolysis, with simple configurations and low material costs, has attained a high readiness level (*4*), but needs a substantial increase in power density (*5-7*). Proton exchange membrane water electrolysis (PEMWE) achieves high efficiency, large current density, and superior dynamic responsiveness (*8-10*), but relies on expensive iridium catalysts to catalyze the sluggish acidic O_2 evolution reaction (OER); moreover, it requires titanium porous

https://doi.org/10.26434/chemrxiv-2023-3zg5f **ORCID:** https://orcid.org/0000-0002-9137-3819 Content not peer-reviewed by ChemRxiv. **License:** CC BY-NC-ND 4.0

transport layers to endure the harsh acidic anode environment (*11-14*). Emerging water electrolysis techniques are moving in two directions. In the pursuit of high power density, bipolar membrane water electrolysis (BPMWE) reduces the activation overpotentials by establishing an acidic environment for H_2 evolution reaction (HER) and a basic environment for OER (*15-18*). Meanwhile, in efforts to lower material cost, membranes or diaphragms are eliminated, via decoupled water splitting that segregates HER and OER in distinct steps (*19-22*), and membrane-less water electrolysis that exploits flow to separate the generated gases (*3, 23-25*). However, a method that can achieve high efficiency at a practical current density with low material costs is currently lacking.

In this work, we propose an unconventional principle of electrochemical water splitting driven by strong electric field in overlapping cathode and anode electric double layers (EDLs). We bring the inter-electrode distance down below the characteristic length of EDLs, resulting in their strong overlap. A pervasive electric field with a strength exceeding 10^7 $V \cdot m^{-1}$ can be established within the overlapping EDLs. This electric field can accelerate the migration of ions across the two electrodes (*26*) and facilitate the dissociation of water molecules (*27*). The electric field enhancement effect has been investigated in fundamental kinetics studies (*28,29*), and applied to electrochemical capacitors (*30*) and sensors (*31-34*). In the realm of water electrolysis, it has been demonstrated that pure water can exhibit a continuous current under the strong electric field in overlapping EDLs (*35*).

H_2 production through water splitting driven by the overlapping EDLs encounters multiple challenges. In addition to technical difficulties in realizing and characterizing the nanoscale overlapping EDLs, a crucial challenge arises from the unwanted crossover of H_2 and O_2 from one electrode to the other, reconverting H_2 and O_2 to water molecules. The gas crossover diminishes the current efficiency and could even lead to a catastrophic failure of H_2 harvesting.

Here, we report a nanofluidic electrolyzer that splits pure water within the overlapping cathode and anode EDLs and effectively improves the current efficiency. Specifically, we introduce convection to the nanochannel between the two confronting electrodes to suppress the crossover of H_2 and O_2. A pair of detector electrodes is embedded downstream of the nanochannel to quantify the H_2 output. The performance of this pure water splitting device is assessed as a function of inter-electrode distance, electrode materials, water flow rate, and the concentration of the electrolyte solution. Mechanistic understanding of the overlapping EDLs is obtained using physical modeling. It is demonstrated that this unconventional electrolysis configuration yields state-of-the-art performance at much-reduced material costs, the nanofluidic electrolyzer offers a promising path to cheap green hydrogen. Aside from electrochemical water splitting, the overlapping EDL is a general strategy to enhance ion transport and tune local reaction conditions.

A nanofluidic reactor for pure water splitting

The nanofluidic reactor consists of two confronting electrodes positioned at a distance that corresponds to the depth of a straight nanochannel in between (Fig. 1A). The nanochannel is interconnected with microchannels through conduits that bridge the gap between micrometer and nanometer scales (Fig. 1B and fig. S1). This scale transition is key for providing convection to the nanochannel. The water flow serves multiple functions, including supplying water, exporting the generated H_2 and O_2, and regulating the gas diffusion boundaries to inhibit the

https://doi.org/10.26434/chemrxiv-2023-3zg5f **ORCID:** https://orcid.org/0000-0002-9137-3819 Content not peer-reviewed by ChemRxiv. **License:** CC BY-NC-ND 4.0

gas crossover (Fig. 1C).

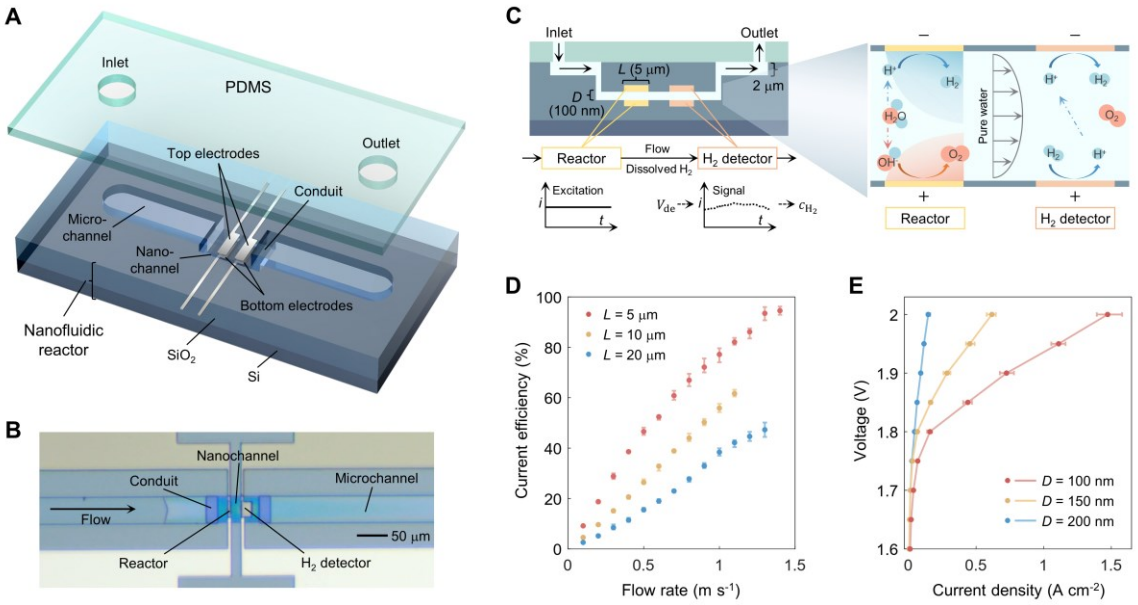

Fig. 1. Nanofluidic reactor for pure water splitting with suppressed gas crossover. (**A**) Schematic diagram of the nanofluidic reactor. Fabricated in a SiO_2 layer on a Si wafer, the nanofluidic reactor features two pairs of confronting platinum (Pt) electrodes. Each pair consists of two electrodes placed on the top and bottom sides of a nanochannel (100 ~ 200 nm in depth). Conduits (500 nm in depth) connect the nanochannel to microchannels (2 μm in depth). The upper ends of the microchannels are sealed by a cube of polydimethylsiloxane (PDMS). (**B**) Top view of the reactor. A liquid water flow is pumped through the microchannel and conduit towards the nanochannel. Movies illustrating the flow can be found in supplementary materials (movie S1-2). (**C**) Cross-sectional side view of the reactor and a schematic diagram showing the respective functions of the two electrode pairs. The upstream confronting electrodes (reactor part) split water into H_2 and O_2, whose concentration distribution (illustrated by gradient colors) and transport are controlled by the rate of the convective flow. The downstream electrodes (H_2 detector part) measure the current signal under a specific voltage (V_{de}) to quantify the current efficiency. D represents the distance of the confronting electrode and the depth of the nanochannel, and L denotes the length of the reactor electrodes along the nanochannel. (**D**) The current efficiency exhibits a positive correlation with the flow rate. The current efficiency was measured at 2 V for the reactor and 0.4 V for the H_2 detector, 20°C and D = 200 nm. (**E**) The performance of pure water splitting improves with decreasing electrode distance. The current density is defined as the ratio of the current of the reactor to the overlapping area of the confronting electrodes ($L \times W$, W denotes the width of the reactor electrodes vertical to the nanochannel). The performance was tested at 60°C, 1 $m \cdot s^{-1}$ flow rate and L = 5 μm, corrected by current efficiency. Notably, gases remained in the dissolved state during measurements of current efficiency and performance.

Detector electrodes are integrated downstream of the same nanochannel to quantify the amount

https://doi.org/10.26434/chemrxiv-2023-3zg5f **ORCID:** https://orcid.org/0000-0002-9137-3819 Content not peer-reviewed by ChemRxiv. **License:** CC BY-NC-ND 4.0

of H_2 output. This proof-of-principle-type design addresses the challenge of detecting dissolved H_2 on the magnitude of picomolar in pure water. The current signal of the detector is amplified due to the reduced ohmic resistance and accelerated H^+ migration from anode to cathode within the overlapping EDLs (Fig. 1C). To address the mixing problem of O_2 and H_2, we meticulously select the voltage of the detector, at which H_2 evolution and oxidation reaction occur at the cathode and anode, respectively, while the electrodes are inert to O_2. We conducted linear sweep voltammetry experiments of the detector in pure water with dissolved H_2, O_2, and N_2 individually. The current of H_2 rises rapidly from 0 V to 0.2 V and remains high thereafter, whereas O_2 reactions occur only above 0.5 V (fig. S2). Thus, we selected 0.4 V as the voltage for the detector. At this voltage, we obtained a linear relationship between the current of the detector and the concentration of dissolved H_2 at various flow rates (fig. S3). This calibrated relationship allows us to determine the amount of H_2 that flows out of the reactor, and subsequently calculate the current efficiency (supplementary text ST-1).

Pure water splitting is realized using the nanofluidic reactor, with the production of H_2 confirmed and the current efficiency quantified by the detector. The current efficiency rises from close to 0% to 95% as the flow rate increases for an electrode length of 5 μm (Fig. 1D). A higher flow rate and a narrower electrode promote the escape of generated gases from the reactor, thus reducing gas crossover to the opposing electrodes. Consequently, after correction of the current efficiency, the current-voltage (IV) curves of pure water splitting are obtained at various distances of the electrodes (Fig. 1E). A 10-fold improvement in the current density at a voltage of 2 V is obtained when the inter-electrode distance decreases from 200 nm to 100 nm. This performance improvement cannot be attributed exclusively to the reduced ohmic resistance at the halved distance. More importantly, it is to be revealed that the performance improvement is caused by changes in ion transport and reaction environments as the overlap of cathode and anode EDLs increases.

Effects of overlapping EDLs

To characterize the overlapping EDLs and understand their effects on pure water splitting, a continuum model is developed. This model, as detailed in supplementary text ST-2, describes ion transport in overlapping EDLs with water electrolysis reactions occurring at the electrode surface. The water dissociation reaction (R_{wd}) is incorporated as a source term in the Poisson-Nernst-Planck equation that describes the transport of H^+ and OH^- in water. Additionally, the model considers the transport of cations M^+ and anions A^- of a supporting electrolyte, if present. The kinetics of HER and OER are described using Butler-Volmer equations in both acidic and basic environments. The potential and ion distributions are simulated within an electrode distance of 100 nm, with and without supporting electrolytes (Fig. 2).

The characteristic length of EDLs, the Debye length, grows from 1 nm in 10^{-1} M acid to 1 μm in pure water (*36*). As the acid concentration decreases, the region of the bulk solution, signified by a plateau in the distribution of electrostatic potential, gradually diminishes (Fig. 2A). In pure water, the potential distribution between cathode and anode is almost linear, indicating an extensive overlap of the EDLs at an inter-electrode distance of 100 nm, namely, one tenth of the Debye length. To quantify the overlap of cathode and anode EDLs, we use the strength of the electric field in the center of the liquid phase as the indicator. We find that it intensifies as the concentration of supporting electrolyte decreases (Fig. 2B). The strong pervasive electric

https://doi.org/10.26434/chemrxiv-2023-3zg5f **ORCID:** https://orcid.org/0000-0002-9137-3819 Content not peer-reviewed by ChemRxiv. **License:** CC BY-NC-ND 4.0

field enhances the capability of ion migration, surpassing the rate required to attain the desired current density of water electrolysis by more than 10^3 times. Conversely, in concentrated solutions with separate EDLs, ion transport relies primarily on diffusion, since migration is weakened by the low electric field in the bulk region of the liquid phase. Moreover, the average ionic strength in the overlapping EDLs increases by a factor of 10^5 in pure water as the applied voltage is increased from 0.2 V to 0.8 V (Fig. 2B). The excess ions are produced from the dissociation of water, driven by the necessity to screen the intense electric field in the absence of sufficient supporting electrolytes. The combined effects of enhanced migration capability and facilitated ionization of water render ion transport between the confronting electrodes in pure water sufficiently close to that in concentrated electrolytes.

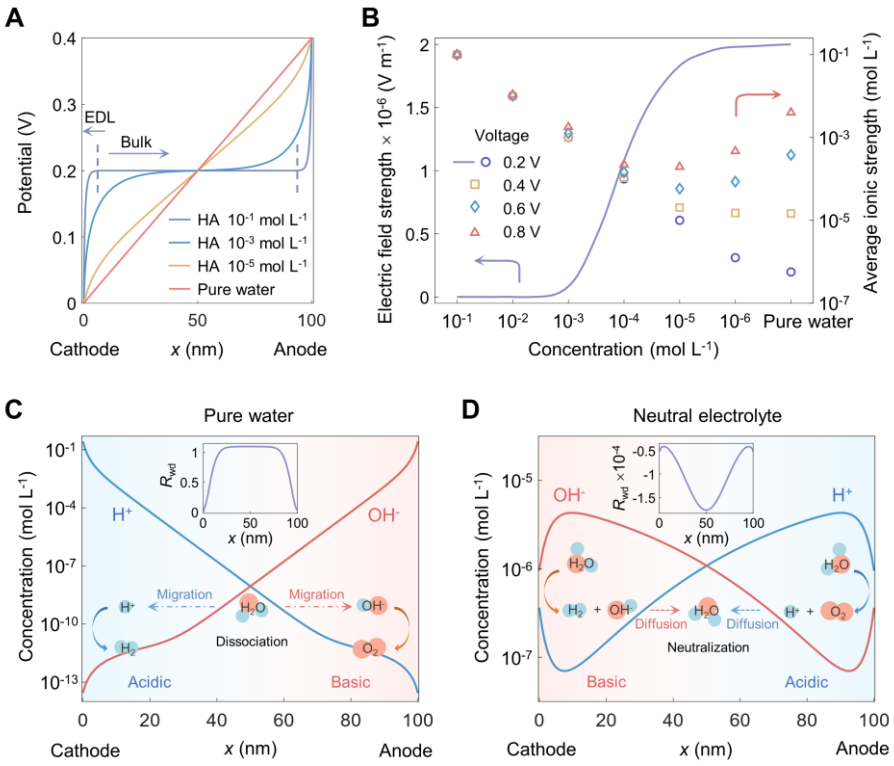

Fig. 2. Electric field enhancement, ionic strength augmentation, and favorable acid-base environment in the overlapping EDLs. (**A**) Distribution of electrostatic potential in electrolyte solution HA (a general denotation for acids with symmetrical ions) at different ion concentrations. The EDLs (demarcated by dashed lines) expand and overlap as the ion concentration decreases. (**B**) Electric field strength at the center of the electrolyte solution and average ionic strength over the whole electrolyte solution of HA (10^{-6} ~ 10^{-1} mol·L^{-1}) and pure water as functions of the applied voltage at an inter-electrode distance of 100 nm. The electric field strength intensifies as the concentration of the supporting electrolyte decreases, caused by the higher degree of EDL overlap. The ionic strength first declines as the ion concentration decreases from 0.1 M to 0.1 mM, but then rises with further decreasing the ion concentration and elevating the voltage difference of the two electrodes. (**C**) An acidic HER and basic OER environment are established during pure water splitting within the overlapping EDLs. The inset shows the net rate of water dissociation R_{wd} (mol·m^{-3}·s^{-1}) in the electrolyte solution, where a

https://doi.org/10.26434/chemrxiv-2023-3zg5f **ORCID:** https://orcid.org/0000-0002-9137-3819 Content not peer-reviewed by ChemRxiv. **License:** CC BY-NC-ND 4.0

positive value indicates the occurrence of water dissociation. (**D**) The concentration distributions of H^+ and OH^- in the electrolysis of a neutral electrolyte reveal a basic HER and acidic OER environment. The inset shows a negative R_{wd}, signifying the occurrence of water neutralization in the electrolyte.

An acidic condition for HER and a basic condition for OER are formed *in situ* in pure water splitting (Fig. 2C). Driven by the electric field in the overlapping EDLs, H^+ and OH^- accumulate near the cathode and anode, respectively, and react on the respective surfaces. Water molecules dissociate in the electrolyte to replenish the consumed ions. In contrast, an opposite environment is formed in the electrolysis with a neutral supporting electrolyte, as predicted in our simulation (Fig. 2D) and seen in experimental studies (*24,37*). In a neutral electrolyte, water molecules dissociate during both electrode reactions, and OH^- and H^+ are generated at the cathode and anode, respectively. These ions subsequently encounter each other in the electrolyte solution and neutralize back to water. The difference in the bipolar reaction environments between pure water and neutral supporting electrolytes is due to the large disparity in ion migration capability within the overlapping and non-overlapping EDLs. In the overlapping EDLs, the strong electric field greatly facilitates the migration of H^+ to the cathode and OH^- to the anode, while in the non-overlapping EDLs, ion transport relies on diffusion driven by concentration gradients (see supplementary text ST-3 and fig. S4 for detailed explanation and factors that influence the acid-base environments). In terms of performance, the co-existence of the favorable acidic and basic environments for HER and OER, respectively, maximizes the reaction activity for pure water splitting.

Our simulation results show that the water dissociation rate in the overlapping EDLs should be accelerated by 6 orders compared to that in bulk water to support a current density as high as 1 $A \cdot cm^2$ (supplementary text ST-2). The acceleration mechanisms are a subject of controversy in literature. The second Wien effect is commonly used to describe the influence of the electric field, which is pronounced when the field strength exceeds 10^8 $V \cdot m^{-1}$ (*38*). Also, molecular dynamics simulations have studied the impact of the electric field on OH bonds within and between water molecules (*39,40*), revealing that water can be autoionized by an electric field higher than 3.5×10^8 $V \cdot m^{-1}$ (*27*). However, the presence of catalysts is considered to be the dominant factor of water dissociation in bipolar membranes (*16,41,42*). Our results indicate that water dissociation can be accelerated without catalysts by an electric field on the magnitude of 10^7 $V \cdot m^{-1}$ (*35,43*). This strength of the electric field does not support water autoionization, yet it can facilitate water dissociation by stretching the OH bond and reorienting water dipoles, resulting in a lower relative permittivity (*44*). Meanwhile, the continuous dissociation is driven by the shift of water balance. In the center of pure water, the concentration of H^+ and OH^- both remain below 10^{-7} M (Fig. 2C), thereby impeding ion recombination. The low concentration of H^+ and OH^- are attributed to the enhanced ion migration in the overlapping EDLs.

Since the overlapping EDLs enhance ion migration and create an acidic HER and basic OER environment, we would expect the electrolytic performance in pure water to be different from that in supporting electrolytes with separate EDLs. Different types and concentrations of electrolytes for water splitting are compared in the nanofluidic reactors (Fig. 3). The performance of acidic electrolysis decreases when the electrolyte concentration decreases from

https://doi.org/10.26434/chemrxiv-2023-3zg5f **ORCID:** https://orcid.org/0000-0002-9137-3819 Content not peer-reviewed by ChemRxiv. **License:** CC BY-NC-ND 4.0

0.5 M to 0.005 M (Fig. 3A). However, pure water splitting outperforms the one with 0.5 M H_2SO_4. Furthermore, a more pronounced difference is observed when comparing pure water splitting with the case of a neutral electrolyte (Fig. 3B). While the neutral electrolyte exhibits no electrolytic current below 2 V, pure water, also originally neutral, initiates electrolysis at voltages below 1.4 V. The high onset potential of the neutral electrolyte is caused by the extra dissociation and neutralization during the basic HER and acidic OER, wasting a thermodynamic potential of 0.83 V (*37,45*). This observation supports the presence of the acidic HER and basic OER during pure water splitting; otherwise, the physics and performance would resemble those of neutral electrolytes.

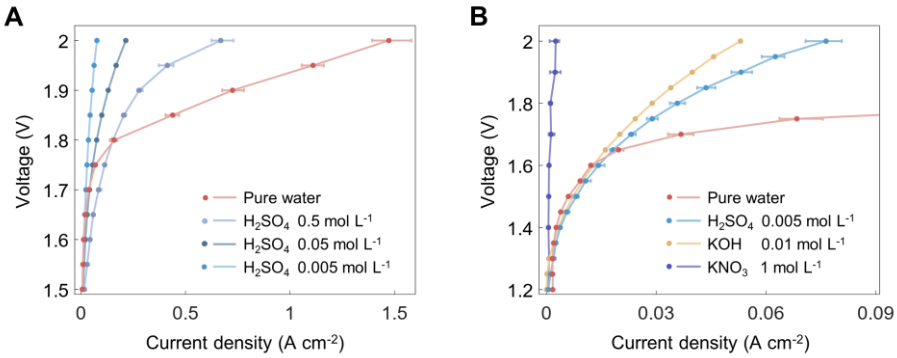

Fig. 3. Performance comparison of pure water and supporting electrolytes in the nanofluidic reactors. (**A**) Pure water splitting outperforms acidic electrolysis. (**B**) Electrolysis with a KNO_3 electrolyte shows negligible electrolytic current below 2 V, while H_2SO_4, KOH, and pure water start to be electrolyzed below 1.4 V, and pure water exhibits superior performance over acid and alkaline electrolytes. The IV curves are measured at 60°C, 1 $m \cdot s^{-1}$ flow rate, D = 100 nm, and L = 5 μm, and corrected by current efficiency.

Notably, the current density of pure water is initially lower than that of 0.5 M H_2SO_4, but becomes higher above 1.8 V (Fig. 3A). This is attributed to the intensified ionic strength in the overlapping EDLs as the voltage is raised (Fig. 2B). Different from conventional electrochemical devices, where the ion concentration and reaction environments are pre-determined by added electrolytes, the present pure-water splitting reactor forms the electrolyte and the bipolar environment *in situ* above a 'voltage threshold'. Subsequently, it exhibits a higher sensitivity to the increase of voltage. This suggests a new approach for electrochemical systems with voltage-tunable ionic strength and local reaction environments. This mechanism also brings another advantage in terms of electrolyte purity, as it circumvents issues related to adsorption, poisoning, and other effects of electrolyte species. Thus, it holds the potential to serve as a platform for various fundamental studies.

Towards high performance with low material cost

Based on the favorable alkaline anode environment in the overlapping EDLs, we replace the Pt anode electrode with ruthenium (Ru) and nickel (Ni) (Fig. 4A). The Ni anode enables a significant improvement in pure-water splitting performance, since Ni possesses a 10^3-fold

https://doi.org/10.26434/chemrxiv-2023-3zg5f **ORCID:** https://orcid.org/0000-0002-9137-3819 Content not peer-reviewed by ChemRxiv. **License:** CC BY-NC-ND 4.0

higher exchange current density under alkaline conditions than Pt (*5*). The residual current observed with the Ru anode at voltages below 1.4 V results from Ru degradation (*46*). Pure water splitting with Ni anode can reach 2.8 A·cm^{-2} at 1.7 V, a performance that surpasses the advanced PEMWE and BPMWE (*8,47,48*).

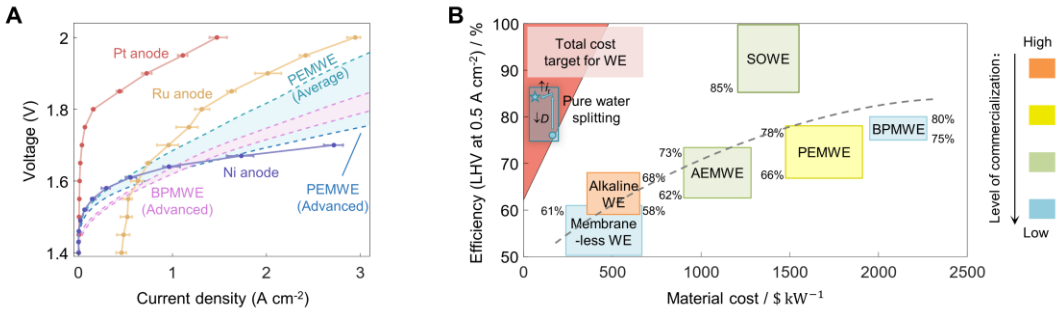

Fig. 4. Ni anode for pure water splitting and comparison with other water electrolysis variants. (**A**) Pure water splitting with Ni and Ru as OER catalysts, which have higher activities in alkaline environments, shows better performance than that with Pt anode. The performance of pure water splitting is measured at 60°C, 1 m·s^{-1} flow rate, D = 100 nm, and L = 5 μm, with current efficiency correction. Pure water splitting with suitable basic OER catalysts provides competitive performance through the comparison with advanced PEMWE and BPMWE, meanwhile, it offers lower material costs due to the absence of membrane and supporting electrolyte, and the potential to use non-precious metal catalysts. (**B**) Targets and status of water electrolyzers. The red triangle represents the requirements of efficiency and material cost to meet the total cost target of water electrolyzers when combined with renewable energy sources at a $0.03 electricity price and 30% capacity factor. The rectangles represent the status and the dashed line summarizes the paradigm of conventional water electrolyzers. The efficiencies and the material costs of the more commercially available methods are analyzed from the literature (*3,4,8,47-51*), while the material costs of the methods in the earlier states are estimated through the comparison among methods. WE denotes water electrolyzer and AEMWE is an acronym for anion exchange membrane WE. The blue dot represents the state of pure water splitting in this work, with an efficiency of 76% at 0.5 A·cm^{-2} and lower material cost than alkaline WE and common membrane-less WE. By reducing the electrode distance (D) and increasing the rated current density (i_r), it is anticipated that the pure water splitting will reach the position of the blue pentagram.

Pure water splitting in the overlapping EDLs delivers competitive electrolysis performance with non-precious materials, which represents a promising path towards low-cost, high-performance water electrolysis. Conventional water electrolyzers typically require supporting electrolytes to enhance the conductivity in the bulk region, such as alkaline water electrolyzers. To further minimize the ohmic resistance, solid electrolytes are employed to reduce the thickness of the bulk. Moreover, achieving higher activity often involves the use of precious metal catalysts, as PEMWE, creating the acid-base environment, as in BPMWE, or raising the temperature above 500°C, as solid oxide water electrolyzers (SOWE). Therefore, those variants are confronted with the challenge of balancing between energy efficiency and material cost,

https://doi.org/10.26434/chemrxiv-2023-3zg5f **ORCID:** https://orcid.org/0000-0002-9137-3819 Content not peer-reviewed by ChemRxiv. **License:** CC BY-NC-ND 4.0

rendering it difficult to meet the overall targets (Fig. 4B; the cost target is analyzed in supplementary text ST-4 and fig. S5).

In contrast, exploiting the effects of overlapping EDLs, pure water splitting achieves state-of-the-art performance without the necessity of membranes, supporting electrolytes, or precious OER catalysts. Moreover, the cathode can also employ earth-abundant materials like MoS_2 to catalyze the acidic HER (*49*). Efficiency can be further enhanced by reducing the electrode distance (*D*). The current density increases more than 10 times when we decrease *D* from 200 nm to 100 nm (Fig. 1E); similar improvements are expected when *D* is further halved to 50 nm with a doubled electric field strength. In a laminated-type reactor with a 50 nm inter-electrode distance, we observe a current density higher than 40 $A \cdot cm^{-2}$ at 2.5 V and 20°C, which demonstrates the potential for efficiency improvement (fig. S6). Meanwhile, increasing the rated current density (i_r) is advantageous for pure water splitting. In Figure 4B, we choose 0.5 $A \cdot cm^{-2}$ as i_r for uniform standard comparison among variants; however, this underestimates the superiority of pure water splitting. 0.5 $A \cdot cm^{-2}$ just barely surpasses the 'voltage threshold' to initiate the ions and environments, as previously discussed (Fig. 3A). Increasing i_r to 3 $A \cdot cm^{-2}$ or higher will lead to a slight decrease in efficiency, but a substantial increase of power density, which will significantly reduce the capacity costs to 30% or less. Consequently, this technique is promising to meet the cost target for H_2 production.

Conclusion

We have reported an unconventional electrochemical water-splitting technology that harnesses the overlapping cathode and anode EDLs to split pure water in a nanofluidic reactor. The crossover of H_2 and O_2 is effectively mitigated by maintaining a sufficient convective flow in the nanochannel. The current efficiency of the reactor has been quantified using a pair of detector electrodes downstream of the channel. The overlap of cathode and anode EDLs gives rise to a pervasive electric field on the magnitude of 10^7 V/m, facilitating water dissociation and ion migration. A 5-order increase in the ion concentration is obtained in pure water, enabling an ionic conductivity comparable to that of a normally concentrated electrolyte. Furthermore, an acidic HER and basic OER environment are formed *in situ* in pure water, reducing the kinetic overpotential for both reactions and enabling the usage of non-precious metal catalysts like Ni. Exploiting the synergy of these factors, a Ni-based pure water reactor can achieve a performance of 2.8 $A \cdot cm^{-2}$ at 1.7 V with no supporting electrolytes. This study constitutes a promising solution for green H_2 production with high energy efficiency at low material cost.

Acknowledgment

H. X. and J.Z thank the financial support from the National Natural Science Foundation of China under grant number 22179069 and Tsinghua University-Toyota Joint Research Center for Hydrogen Energy and Fuel Cell Technology of Vehicle (20233930064). J.H. is supported by the Initiative and Networking Fund of the Helmholtz Association (No. VH-NG-1709). M.E. acknowledges financial support from Forschungszentrum Jülich GmbH, received within the framework of the Helmholtz program Materials and Technologies for the Energy Transportation under the Topic Chemical Energy Carriers and the Subtopic Electrochemistry for hydrogen.

https://doi.org/10.26434/chemrxiv-2023-3zg5f **ORCID:** https://orcid.org/0000-0002-9137-3819 Content not peer-reviewed by ChemRxiv. **License:** CC BY-NC-ND 4.0

Reference

1. S. J. Davis et al., Net-zero emissions energy systems. *Science* **360**, eaas9793 (2018). DOI: 10.1126/science.aas9793.
2. J. Chi, H. Yu, Water electrolysis based on renewable energy for hydrogen production. *Chinese Journal of Catalysis* **39**, 390-394 (2018). DOI: 10.1016/S1872-2067(17)62949-8.
3. D. V. Esposito, Membraneless electrolyzers for low-cost hydrogen production in a renewable energy future. *Joule* **1**, 651-658 (2017). DOI: 10.1016/j.joule.2017.11.013.
4. A. Buttler, H. Spliethoff, Current status of water electrolysis for energy storage, grid balancing and sector coupling via power-to-gas and power-to-liquids: A review. *Renewable and Sustainable Energy Reviews* **82**, 2440-2454 (2018). DOI: 10.1016/j.rser.2017.09.003.
5. K. Zeng, D. Zhang, Recent progress in alkaline water electrolysis for hydrogen production and applications. *Progress in energy and combustion science* **36**, 307-326 (2010). DOI: 10.1016/j.pecs.2009.11.002.
6. R. Phillips, C. W. Dunnill, Zero gap alkaline electrolysis cell design for renewable energy storage as hydrogen gas. *RSC advances* **6**, 100643-100651 (2016). DOI: 10.1039/c6ra22242k.
7. M. T. de Groot, A. W. Vreman, Ohmic resistance in zero gap alkaline electrolysis with a Zirfon diaphragm. *Electrochimica Acta* **369**, 137684 (2021). DOI: 10.1016/j.electacta.2020.137684.
8. M. Carmo, D. L. Fritz, J. Mergel, D. Stolten, A comprehensive review on PEM water electrolysis. *International journal of hydrogen energy* **38**, 4901-4934 (2013). DOI: 10.1016/j.ijhydene.2013.01.151.
9. M. Bernt, H. A. Gasteiger, Influence of ionomer content in IrO2/TiO2 electrodes on PEM water electrolyzer performance. *Journal of The Electrochemical Society* **163**, F3179 (2016). DOI: 10.1149/2.0231611jes.
10. R. T. Liu, Z. L. Xu, F. M. Li, F. Y. Chen, J. Y. Yu, Y. Yan, Y. Chen, B. Y. Xia, Recent advances in proton exchange membrane water electrolysis. *Chemical Society Reviews* **52**, 5652-5683 (2023). DOI: 10.1039/D2CS00681B.
11. I. Katsounaros, S. Cherevko, A. R. Zeradjanin, K. J. Mayrhofer, Oxygen electrochemistry as a cornerstone for sustainable energy conversion. *Angewandte Chemie International Edition* **53**, 102-121 (2014). DOI: 10.1002/anie.201306588.
12. M. Bernt, A. Siebel, H. A. Gasteiger, Analysis of voltage losses in PEM water electrolyzers with low platinum group metal loadings. *Journal of The Electrochemical Society* **165**, F305-F314 (2018). DOI: 10.1149/2.0641805jes.
13. Y. Chen, C. Liu, J. Xu, C. Xia, P. Wang, B. Y. Xia, Y. Yan, X. Wang, Key components and design strategy for a proton exchange membrane water electrolyzer. *Small Structures* **4**, 2200130 (2023). DOI: 10.1002/sstr.202200130.
14. Q. Feng, G. Liu, B. Wei, Z. Zhang, H. Li, H. Wang, A review of proton exchange membrane water electrolysis on degradation mechanisms and mitigation strategies.

https://doi.org/10.26434/chemrxiv-2023-3zg5f **ORCID:** https://orcid.org/0000-0002-9137-3819 Content not peer-reviewed by ChemRxiv. **License:** CC BY-NC-ND 4.0

Journal of Power Sources **366**, 33-55 (2017). DOI: 10.1016/j.jpowsour.2017.09.006.

15. Z. Yan, L. Zhu, Y. C. Li, R. J. Wycisk, P. N. Pintauro, M. A. Hickner, T. E. Mallouk, The balance of electric field and interfacial catalysis in promoting water dissociation in bipolar membranes. *Energy & Environmental Science* **11**, 2235-2245 (2018). DOI: 10.1039/c8ee01192c.

16. S. Z. Oener, M. J. Foster, S. W. Boettcher, Accelerating water dissociation in bipolar membranes and for electrocatalysis. *Science* **369**, 1099-1103 (2020). DOI: 10.1126/science.aaz1487.

17. S. Z. Oener, L. P. Twight, G. A. Lindquist, S. W. Boettcher, Thin cation-exchange layers enable high-current-density bipolar membrane electrolyzers via improved water transport. *ACS Energy Letters* **6**, 1-8 (2020). DOI: 10.1021/acsenergylett.0c02078.

18. E. J. Park, C. G. Arges, H. Xu, Y. S. Kim, Membrane strategies for water electrolysis. *ACS Energy Letters* **7**, 3447-3457 (2022). DOI: 10.1021/acsenergylett.2c01609.

19. B. Rausch, M. D. Symes, G. Chisholm, L. Cronin, Decoupled catalytic hydrogen evolution from a molecular metal oxide redox mediator in water splitting. *Science* **345**, 1326-1330 (2014). DOI: 10.1126/science.1257443.

20. H. Dotan, A. Landman, S. W. Sheehan, K. D. Malviya, G. E. Shter, D. A. Grave, Z. Arzi, N. Yehudai, M. Halabi, N. Gal, N. Hadari, C. Cohen, A. Rothschild, G. S. Grader, Decoupled hydrogen and oxygen evolution by a two-step electrochemical–chemical cycle for efficient overall water splitting. *Nature Energy* **4**, 786-795 (2019). DOI: 10.1038/s41560-019-0462-7.

21. P. J. McHugh, A. D. Stergiou, M. D. Symes, Decoupled electrochemical water splitting: from fundamentals to applications. *Advanced Energy Materials* **10**, 2002453 (2020). DOI: 10.1002/aenm.202002453.

22. M. Vanags, G. Kulikovskis, J. Kostjukovs, L. Jekabsons, A. Sarakovskis, K. Smits, L. Bikse, A. Šutka, Membrane-less amphoteric decoupled water electrolysis using WO 3 and Ni (OH) 2 auxiliary electrodes. *Energy & Environmental Science* **15**, 2021-2028 (2022). DOI: 10.1039/d1ee03982b.

23. S. M. H. Hashemi, M. A. Modestino, D. Psaltis, A membrane-less electrolyzer for hydrogen production across the pH scale. *Energy & Environmental Science* **8**, 2003-2009 (2015). DOI: 10.1039/c5ee00083a.

24. O. O. Talabi, A. E. Dorfi, G. D. O'Neil, D. V. Esposito, Membraneless electrolyzers for the simultaneous production of acid and base. *Chemical Communications* **53**, 8006-8009 (2017). DOI: 10.1039/c7cc02361h.

25. K. Deng, H. Feng, Y. Zhang, D. Liu, Q. Li, Ampere-level membrane-less water electrolysis enabled by rose-petal-effect-mimetic interface. *Joule* **7**, 1852-1866 (2023). DOI: 10.1016/j.joule.2023.06.010.

26. M. Jaugstetter, N. Blanc, M. Kratz, K. Tschulik, Electrochemistry under confinement. *Chemical Society Reviews* **51**, 2491-2543 (2022). DOI: 10.1039/d1cs00789k.

27. A. M. Saitta, F. Saija, P. V. Giaquinta, Ab initio molecular dynamics study of dissociation

https://doi.org/10.26434/chemrxiv-2023-3zg5f **ORCID:** https://orcid.org/0000-0002-9137-3819 Content not peer-reviewed by ChemRxiv. **License:** CC BY-NC-ND 4.0

of water under an electric field. *Physical review letters* **108**, 207801 (2012). DOI: 10.1103/PhysRevLett.108.207801.

28. M. A. Zevenbergen, B. L. Wolfrum, E. D. Goluch, P. S. Singh, S. G. Lemay, Fast electron-transfer kinetics probed in nanofluidic channels. *Journal of the American Chemical Society* **131**, 11471-11477 (2009). DOI: 10.1021/ja902331u.

29. J. H. Bae, Y. Yu, M. V. Mirkin, Diffuse layer effect on electron-transfer kinetics measured by scanning electrochemical microscopy (SECM). *The Journal of Physical Chemistry Letters* **8**, 1338-1342 (2017). DOI: 10.1021/acs.jpclett.7b00161.

30. Y. Hu, M. Wu, F. Chi, G. Lai, P. Li, W. He, B. Lu, C. Weng, J. Lin, F. Chen, H. Cheng, F. Liu, L. Jiang, L. Qu, (2023). Ultralow-resistance electrochemical capacitor for integrable line filtering. *Nature* **624**, 74–79 (2023). DOI: 10.1038/s41586-023-06712-2.

31. C. Ma, N. M. Contento, P. W. Bohn, Redox cycling on recessed ring-disk nanoelectrode arrays in the absence of supporting electrolyte. *Journal of the American Chemical Society* **136**, 7225-7228 (2014). DOI: 10.1021/ja502052s.

32. J. Xiong, Q. Chen, M. A. Edwards, H. S. White, Ion transport within high electric fields in nanogap electrochemical cells. *ACS nano* **9**, 8520-8529 (2015). DOI: 10.1021/acsnano.5b03522.

33. Q. Chen, K. McKelvey, M. A. Edwards, H. S. White, Redox cycling in nanogap electrochemical cells. The role of electrostatics in determining the cell response. T*he Journal of Physical Chemistry C* **120**, 17251-17260 (2016). DOI: 10.1021/acs.jpcc.6b05483.

34. S. R. Kwon, K. Fu, D. Han, P. W. Bohn, Redox cycling in individually encapsulated attoliter-volume nanopores. *ACS nano* **12**, 12923-12931 (2018). DOI: 10.1021/acsnano.8b08693.

35. Y. Wang, S. R. Narayanan, W. Wu, Field-assisted splitting of pure water based on deep-sub-debye-length nanogap electrochemical cells. *ACS nano* **11**, 8421-8428 (2017). DOI: 10.1021/acsnano.7b04038.

36. J. Huang, Y. Chen, M. Eikerling, Correlated surface-charging behaviors of two electrodes in an electrochemical cell. *Proceedings of the National Academy of Sciences* **120**, e2307307120 (2023). DOI: 10.1073/pnas.2307307120.

37. G. D. O'Neil, C. D. Christian, D. E. Brown, D. V. Esposito, Hydrogen production with a simple and scalable membraneless electrolyzer. *Journal of The Electrochemical Society* **163**, F3012 (2016). DOI: 10.1149/2.0021611jes.

38. L. Onsager, Deviations from Ohm's law in weak electrolytes. *The Journal of chemical physics* **2**, 599-615 (1934). DOI: 10.1063/1.1749541.

39. P. L. Geissler, C. Dellago, D. Chandler, J. Hutter, M. Parrinello, Autoionization in liquid water. *Science* **291**, 2121-2124 (2001). DOI: 10.1126/science.1056991.

40. M. Moqadam, A. Lervik, E. Riccardi, V. Venkatraman, B. K. Alsberg, T. S. van Erp, Local initiation conditions for water autoionization. *Proceedings of the National Academy of Sciences* **115**, E4569-E4576 (2018). DOI: 10.1073/pnas.1714070115.

https://doi.org/10.26434/chemrxiv-2023-3zg5f **ORCID:** https://orcid.org/0000-0002-9137-3819 Content not peer-reviewed by ChemRxiv. **License:** CC BY-NC-ND 4.0

41. H. Strathmann, J. J. Krol, H. J. Rapp, G. Eigenberger, Limiting current density and water dissociation in bipolar membranes. *Journal of Membrane Science* **125**, 123-142 (1997). DOI: 10.1016/S0376-7388(96)00185-8.

42. L. Chen, Q. Xu, S. Z. Oener, K. Fabrizio, S. W. Boettcher, Design principles for water dissociation catalysts in high-performance bipolar membranes. *Nature communications* **13**, 3846 (2022). DOI: 10.1038/s41467-022-31429-7.

43. A. R. Rezk, H. Ahmed, T. L. Brain, J. O. Castro, M. K. Tan, J. Langley, N. Cox, J. Mondal, W. Li, M. Ashokkumar, L. Y. Yeo, Free radical generation from high-frequency electromechanical dissociation of pure water. *The journal of physical chemistry letters* **11**, 4655-4661 (2020). DOI: 10.1021/acs.jpclett.0c01227.

44. R. M. Adar, T. Markovich, A. Levy, H. Orland, D. Andelman, Dielectric constant of ionic solutions: Combined effects of correlations and excluded volume. *The Journal of chemical physics* **149** (2018). DOI: 10.1063/1.5042235.

45. Y. Ding, P. Cai, Z. Wen, Electrochemical neutralization energy: from concept to devices. *Chemical Society Reviews* **50**, 1495-1511 (2021). DOI: 10.1039/d0cs01239d.

46. A. V. Marenich, A. Majumdar, M. Lenz, C. J. Cramer, D. G. Truhlar, Construction of Pourbaix Diagrams for Ruthenium-Based Water-Oxidation Catalysts by Density Functional Theory. *Angewandte Chemie International Edition* **51**, 12810-12814 (2012). DOI: 10.1002/anie.201206012.

47. K. A. Lewinski, D. van der Vliet, S. M. Luopa, NSTF advances for PEM electrolysis-the effect of alloying on activity of NSTF electrolyzer catalysts and performance of NSTF based PEM electrolyzers. *Ecs Transactions* **69**, 893 (2015). DOI: 10.1149/06917.0893ecst.

48. B. Mayerhöfer, D. McLaughlin, T. Böhm, M. Hegelheimer, D. Seeberger, S. Thiele, Bipolar membrane electrode assemblies for water electrolysis. *ACS applied energy materials* **3**, 9635-9644 (2020). DOI: 10.1021/acsaem.0c01127.

49. G. Li, D. Zhang, Y. Yu, S. Huang, W. Yang, L. Cao, Activating MoS2 for pH-universal hydrogen evolution catalysis. *Journal of the American Chemical Society* **139**, 16194-16200 (2017). DOI: 10.1021/jacs.7b07450.

50. M. I. Gillespie, F. Van Der Merwe, R. J. Kriek, Performance evaluation of a membraneless divergent electrode-flow-through (DEFT) alkaline electrolyser based on optimisation of electrolytic flow and electrode gap. *Journal of Power Sources* **293**, 228-235 (2015). DOI: 10.1016/j.jpowsour.2015.05.077.

51. I. Vincent, D. Bessarabov, Low cost hydrogen production by anion exchange membrane electrolysis: A review. *Renewable and Sustainable Energy Reviews* **81**, 1690-1704 (2018). DOI: 10.1016/j.rser.2017.05.258.

52. Y. Tanaka, Water dissociation reaction generated in an ion exchange membrane. *Journal of Membrane Science* **350**, 347-360 (2010). DOI: 10.1016/j.memsci.2010.01.010.

53. N. Agmon, H. J. Bakker, R. K. Campen, R. H. Henchman, P. Pohl, S. Roke, M. Thämer, A. Hassanali, Protons and hydroxide ions in aqueous systems. *Chemical reviews* **116**, 7642-7672 (2016). DOI: 10.1021/acs.chemrev.5b00736.

https://doi.org/10.26434/chemrxiv-2023-3zg5f **ORCID:** https://orcid.org/0000-0002-9137-3819 Content not peer-reviewed by ChemRxiv. **License:** CC BY-NC-ND 4.0

54. Y. Zheng, Y. Jiao, A. Vasileff, S. Z. Qiao, The hydrogen evolution reaction in alkaline solution: from theory, single crystal models, to practical electrocatalysts. *Angewandte Chemie International Edition* **57**, 7568-7579 (2018). DOI: 10.1002/anie.201710556.

55. T. J. Schmidt, P. N. Ross Jr, N. M. Markovic, Temperature dependent surface electrochemistry on Pt single crystals in alkaline electrolytes: Part 2. The hydrogen evolution/oxidation reaction. *Journal of Electroanalytical Chemistry* **524**, 252-260 (2002). DOI: 10.1016/S0022-0728(02)00683-6.

https://doi.org/10.26434/chemrxiv-2023-3zg5f **ORCID:** https://orcid.org/0000-0002-9137-3819 Content not peer-reviewed by ChemRxiv. **License:** CC BY-NC-ND 4.0